A Steerable Dyadic Wavelet Transform and Interval Wavelets for Enhancement of Digital Mammography

Andrew Laine, Iztok Koren, Wuhai Yang, and Fred Taylor

Computer and Information Sciences Department
Computer Science and Engineering Building, Room 301
University of Florida
Gainesville, FL 32611-2024
Email: laine@cis.ufl.edu, Phone: (904) 392-1239

ABSTRACT

This paper describes two approaches for accomplishing interactive feature analysis by overcomplete multiresolution representations. We show quantitatively that transform coefficients, modified by an adaptive non-linear operator, can make more obvious unseen or barely seen features of mammography without requiring additional radiation. Our results are compared with traditional image enhancement techniques by measuring the local contrast of known mammographic features.

We design a filter bank representing a steerable dyadic wavelet transform that can be used for multiresolution analysis along arbitrary orientations. Digital mammograms are enhanced by orientation analysis performed by a steerable dyadic wavelet transform. Arbitrary regions of interest (ROI) are enhanced by Deslauriers-Dubuc interpolation representations on an interval. We demonstrate that our methods can provide radiologists with an interactive capability to support localized processing of selected (suspicious) areas (lesions).

Features extracted from multiscale representations can provide an adaptive mechanism for accomplishing local contrast enhancement. By improving the visualization of breast pathology we can improve chances of early detection while requiring less time to evaluate mammograms for most patients.

Keywords: Multiresolution analysis, dyadic wavelets, image enhancement, non-linear operators.

1. INTRODUCTION

Many cancers escape detection due to the density of surrounding breast tissue. For example, differences in attenuation of the various soft tissue structures in the female breast are small, and it is necessary to use low levels of X-ray energy to obtain high contrast in mammographic film. Since contrast between the soft tissues of the breast is inherently low and because relatively minor changes in mammary structure can signify the presence of a malignant breast tumor, the detection is more difficult in mammography than in most other forms of radiography. The radiologist must search for malignancy in mammographic features such as microcalcifications, dominate and stellate masses, as well as textures of fibrous tissues (fibroglandular patterns).

Analyzing images along distinct orientations and resolutions is advantageous in many computational vision and image processing tasks. Filtering in a continuum of orientations [1] or other deformations [2, 3] can be performed by combining outputs of a finite set of filters. Such a scheme can be employed for decomposition/reconstruction as well: a pyramid implemented as a near-perfect reconstruction filter bank was previously designed in [4]. We present a filter bank implementation of a discrete dyadic wavelet transform that is constructed to make possible analysis along arbitrary orientations. We demonstrate the effectiveness of our scheme for the enhancement of digital mammography.

We shall present a novel method for accomplishing an interactive paradigm for adaptive contrast enhancement [14, 15, 16, 17, 18]. We describe a method of image enhancement that uses Deslauriers-Dubuc

0-8194-1844-7/95/$6.00

interpolation wavelets [11, 13] on intervals to compute multiscale representations. Mammograms are then reconstructed from transform coefficients modified at each level by local and global non-linear operators.

This can provide radiologists with an interactive capability for processing large digital mammograms with selected ROI's enhanced and displayed on the screen. In this paper, we show preliminary results that demonstrate the efficiency of such methods for digital mammography.

2. IMAGE ENHANCEMENT USING STEERABLE DYADIC WAVELETS

2.1 STEERABLE FILTERS

Freeman et al. [1] proposed an efficient scheme for computing arbitrary rotations of a two-dimensional (2-D) function. A function rotated by an arbitrary angle was formulated as a linear combination of basis functions. Using polar coordinates ($r = \sqrt{x^2 + y^2}$ and $\phi = \arg(x, y)$) we can write

$$F(r, \phi - \phi_0) \;=\; \sum_{m=1}^{M} k_m(\phi_0)\, B(r, \phi - \phi_m), \tag{1}$$

where $F(r, \phi)$ is an original function, ϕ_0 denotes an arbitrary rotation, $\{k_m(\phi_0)\}$ is a set of interpolation functions, $\{B(r, \phi - \phi_m)\}$ is a set of basis functions, and $\{\phi_m\}$ is a set of constants.

If $F(r, \phi)$ represents a frequency response, the result of filtering with a rotated frequency response $F(r, \phi - \phi_0)$ can be computed simply by $\{k_m(\phi_0)\}$ weighted linear combination of outputs from filters $\{B(r, \phi - \phi_m)\}$. When a large number of rotations of a template filter is required, the above scheme can lead to substantial savings in both computational speed and memory consumption.

Not every function $F(r, \phi)$, however, can be expressed as a finite sum shown in Eq. 1. In fact [1], there is a finite number of terms in Eq. 1 only when $F(r, \phi)$ has a finite number of terms in the Fourier series expansion in polar angle ϕ:

$$F(r, \phi) \;=\; \sum_{n=-N}^{N} a_n(r)\, e^{jn\phi}, \tag{2}$$

where j stands for $\sqrt{-1}$.

In [1] functions having a finite number of terms in Eq. 2 were called "steerable" and the minimum number of basis functions sufficient to "steer" $F(r, \phi)$ (i.e., the minimum number of terms in Eq. 1) was equal to the number of nonzero coefficients in the Fourier series expansion of Eq. 2.

Solving for the interpolation functions in Eq. 1 with $B(r, \phi - \phi_m) = F(r, \phi - \phi_m)$ yields the system [1]

$$\begin{bmatrix} 1 \\ e^{j\phi_0} \\ \vdots \\ e^{jN\phi_0} \end{bmatrix} = \begin{bmatrix} 1 & 1 & \cdots & 1 \\ e^{j\phi_1} & e^{j\phi_2} & \cdots & e^{j\phi_M} \\ \vdots & \vdots & & \vdots \\ e^{jN\phi_1} & e^{jN\phi_2} & \cdots & e^{jN\phi_M} \end{bmatrix} \begin{bmatrix} k_1(\phi_0) \\ k_2(\phi_0) \\ \vdots \\ k_M(\phi_0) \end{bmatrix}. \tag{3}$$

The frequencies in the left-hand side vector of Eq. 3 correspond to the non-negative frequencies of Eq. 2. For coefficients $a_n = 0$ the rows corresponding to each n are removed from the matrix formulation shown in Eq. 3.

2.2. A STEERABLE DYADIC WAVELET TRANSFORM

To design a steerable dyadic wavelet transform we imposed the additional constraint of polar separability on the function $F(r, \phi)$:

$$F(r, \phi) \;=\; F_R(r)\, F_\Phi(\phi). \tag{4}$$

Using Eq. 4 and $B(r, \phi - \phi_m) = F(r, \phi - \phi_m)$ Eq. 1 then becomes

$$F_\Phi(\phi - \phi_0) \;=\; \sum_{m=1}^{M} k_m(\phi_0)\, F_\Phi(\phi - \phi_m), \tag{5}$$

The radial portion of function $F(r, \phi)$ is thus no longer a part of the steering constraint and can be designed separately. Similar to the method described in [4] we first designed radial portions of our filters and then applied any desired angular variation.

We selected a dyadic wavelet transform [5], with which we had previously obtained promising results for mammographic feature enhancement [18]. Instead of using the dyadic wavelet transform in its separable form as originally proposed, we constructed a nonseparable 2-D dyadic wavelet transform. This was accomplished by designing circularly symmetric filters from a filter bank implementation of a fast algorithm for computing a 1-D discrete dyadic wavelet transform [5]. Figure 1 shows the filter bank implementation of the one-dimensional discrete dyadic wavelet transform used for the design of the radial component.

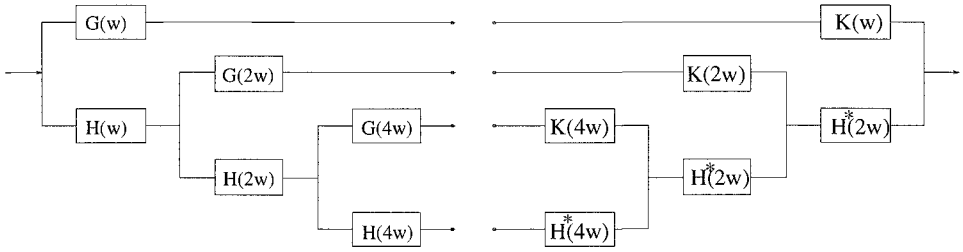

Figure 1: Computational structure for a one-dimensional discrete dyadic wavelet transform used for computing radial components (three levels shown).

To map a 1-D filter frequency response into a 2-D circularly symmetric frequency response and obtain a real 2-D filter impulse response, the 1-D filter frequency response should be real. Thus, from the family of filters proposed in [5] we choose

$$\begin{aligned} H(\omega) &= \left[\cos\left(\frac{\omega}{2}\right)\right]^2, \\ G(\omega) &= -4\left[\sin\left(\frac{\omega}{2}\right)\right]^2, \\ K(\omega) &= \frac{1-|H(\omega)|^2}{G(\omega)}. \end{aligned} \tag{6}$$

Mammographic features may occur in any orientation. Thus we desired our 2-D filters to be circularly symmetric over the entire frequency domain, and choose the 2-D frequency response to be

$$F_R(\omega_x, \omega_y) = \begin{cases} F(\omega_R) & \text{if } \omega_R < \pi \\ F(\pi) & \text{otherwise,} \end{cases}$$

where $\omega_R = \sqrt{\omega_x^2 + \omega_y^2}$ and $F(\omega)$ was one of the filters defined previously in Eq. 6.

Since it is difficult to estimate values of the 2-D frequency response for $\omega_R > \pi$, we clipped the frequency response in this region to the value of the 1-D frequency response at π.

Thus, the frequency responses of the constructed 2-D filters in the radial direction matched the frequency responses of their 1-D counterparts. Impulse responses, however, did not match (even for the continuous case the circularly symmetric frequency response and the corresponding circularly symmetric impulse response are not related in the radial direction by Fourier, but rather by the Hankel transform [6]). The impulse responses of the resulting 2-D filters were not compactly supported, but the magnitudes of the coefficients decreased quickly away from the maximum magnitude coefficient, making the impulse responses suitable for truncation and windowing.

Figure 2 shows circularly symmetric magnitude frequency responses of 2-D filters $H_R(\omega_x, \omega_y)$, $G_R(\omega_x, \omega_y)$, and $K_R(\omega_x, \omega_y)$.

For the angular portion of the frequency response we choose from the family of functions

$$G_\Phi(\phi) = \begin{cases} \cos^n(\phi) & \text{for } n \text{ even} \\ j\cos^n(\phi) & \text{for } n \text{ odd.} \end{cases} \tag{7}$$

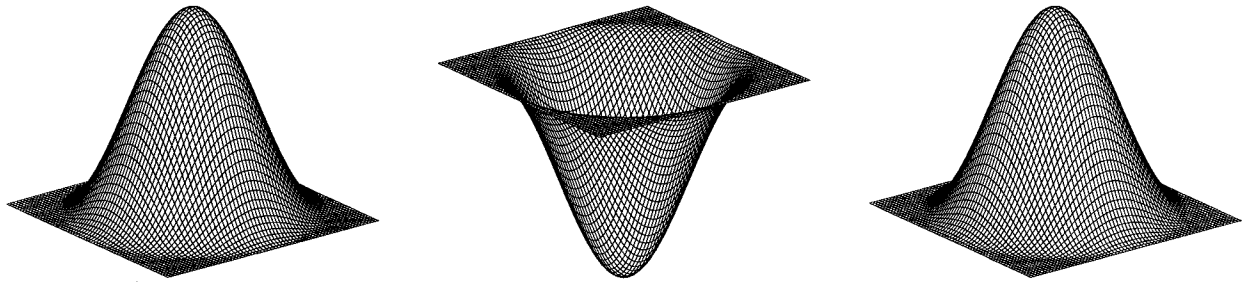

Figure 2: Circularly symmetric magnitude frequency responses of filters $H_R(\omega_x, \omega_y)$, $G_R(\omega_x, \omega_y)$, and $K_R(\omega_x, \omega_y)$.

For large values of n, better angular resolution of the filter was possible. The minimum number of basis functions required to steer the function $G_\Phi(\phi)$ was equal to $n+1$. When solving Eq. 3 we choose $\{\phi_m\}$ equally spaced between 0 and π.

Thus the filters were formulated by

$$\begin{aligned} H(\omega_x, \omega_y) &= H_R(\omega_x, \omega_y) \\ G(\omega_x, \omega_y) &= G_R(\omega_x, \omega_y)\, G_\Phi(\phi), \text{ and} \\ K(\omega_x, \omega_y) &= K_R(\omega_x, \omega_y). \end{aligned}$$

The frequency response of filters $H(\omega_x, \omega_y)$ and $K(\omega_x, \omega_y)$ were circularly symmetric, while the frequency response of filter $G(\omega_x, \omega_y)$ was a product of radial and angular portions. Figure 3 shows the magnitude frequency responses of filter $G(\omega_x, \omega_y)$ with $n = 2$ in Eq. 7 and $\{\phi_m\}=\{0, \frac{\pi}{3}, \frac{2\pi}{3}\}$ in Eq. 5.

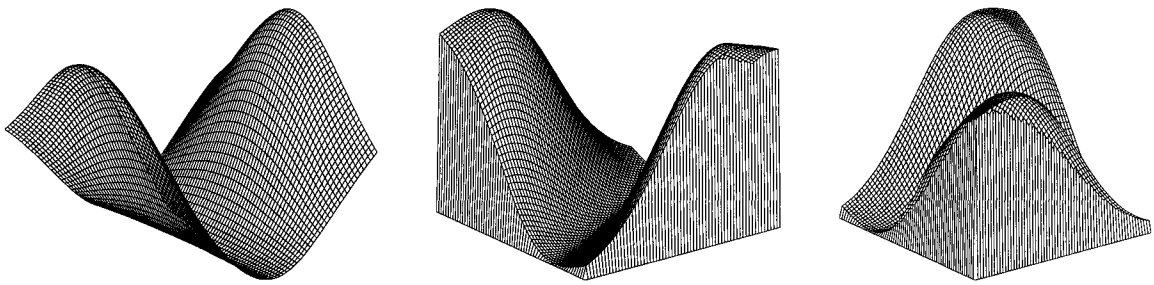

Figure 3: The magnitude frequency responses of filter $G(\omega_x, \omega_y)$.

2.3. IMAGE ENHANCEMENT

To enhance an image, wavelet coefficients were modified by a nonlinear enhancement function [7]:

$$E(x) = \begin{cases} x - (K-1)T & \text{if } x < -T \\ Kx & \text{if } |x| \le T \\ x + (K-1)T & \text{if } x > T. \end{cases} \tag{8}$$

As in [4] we steer the filters G to a local dominant orientation at each scale and position. Coefficients are then modified by computing the maximum oriented energy and Eq. 8. The filters are then steered back to their original orientations, and reconstruction from the modified coefficients is then carried out.

We find the local dominant orientation from the outputs of quadrature filters (i.e., filters that are Hilbert transform pairs). The Hilbert transform of Eq. 7 is

$$G_{\Phi_H}(\phi) = \begin{cases} -j\,\mathrm{sgn}(\cos(\phi))\cos^n(\phi) & \text{for } n \text{ even} \\ |\cos^n(\phi)| & \text{for } n \text{ odd}, \end{cases} \tag{9}$$

where

$$\mathrm{sgn}(x) = \begin{cases} 1 & \text{if } x \geq 0 \\ -1 & \text{if } x < 0. \end{cases}$$

Functions $G_{\Phi_H}(\phi)$ in Eq. 9 are not steerable. We approximated them with truncated Fourier series expansion using only a few maximum-magnitude coefficients.

The oriented energy was defined by

$$En(\phi_0) = \left(G^{\phi_0}\right)^2 + \left(G_H^{\phi_0}\right)^2, \tag{10}$$

with G^{ϕ_0} being the output of the filter $G(r, \phi - \phi_0)$ and $G_H^{\phi_0}$ the output of its Hilbert transform.

To estimate the orientation that maximizes Eq. 10 in case of only a single local orientation, we follow [1]: $En(\phi_0)$ is expanded into a Fourier trigonometric series

$$En(\phi_0) = a_0 + a_2 \cos(2\phi_0) + b_2 \sin(2\phi_0) + \ldots$$

Then the orientation $\phi_{0_{max}}$ and magnitude $M = En(\phi_{0_{max}})$ were approximated by

$$\phi_{0_{max}} = \frac{\text{argument}(a_2 + jb_2)}{2}$$

$$M = \sqrt{a_2^2 + b_2^2}.$$

Figure 4 shows an original mammographic image, the image filtered by a set of basis filters at different scales, and the enhanced image. Eqs. 7 and 9 were used with $n = 3$, and Eqs. 8 with $K = 20$, $T = 0.2$. We observed that the oriented structure is made more visible in the enhanced image.

3. LOCAL FEATURE ANALYSIS VIA INTERVAL WAVELETS

3.1 FRAMEWORK

In this part of the paper, we investigated multiresolution representations of Dubuc-Delauriers interpolation wavelets[11, 13].This representation was attractive because it overcame "edge effects" of traditional multiresolution representations (based on perodization of a finite signal to a signal on a line; or simply adding zeros to extend a signal on a line). The shape of the basis functions of this representation was symmetric or antisymmetric, and allowed for perfect reconstruction . We have applied this representation to decompose an arbitrary region of interest of a mammogram, so that a selected region may be analyzed independently.

In many applications, a signal has finite length, such that the signal lives on the interval $[0, 1]$, or in the two dimmensional case, an image. Cohen and Daubechies [8] and Jawerth and Sweldens [9] adapted multiresoluton analysis on the line to "life on the interval", where a sequence of successive approximation spaces on the interval were constructed as: $\overline{\bigcup_{j\in\mathbf{Z}} V_j} = \mathbf{L}^2[0,1]$, $\bigcap_{j\in\mathbf{Z}} V_j = \{0\}$. By defining W_j as an orthogonal complement of V_j in V_{j-1}, $V_{j-1} = V_j \bigoplus W_j$, the space $\mathbf{L}^2[0,1]$ can be representd as a direct sum $\mathbf{L}^2[0,1] = \bigoplus_{j\in\mathbf{Z}} W_j$.

3.1.1. Deslauriers-Dubuc interpolation

We considered multiresolution representations of the Deslauriers-Dubuc fundamental functions [11, 13]. Figure 6 shows the fundamental solution of Deslauriers-Dubuc interpolation and associated wavelets ($D = 3$).

Donoho [12] showed how to adapt the Deslauriers-Dubuc interpolating transform to "life on the interval". Suppose that $\phi_{j,k}$ is a scaling function on the line. The scaling functions on the interval $\psi_{j,k}^{interv}$ can be derived by: (1) within the *interior* of the interval, they are defined the same as on the real line

$$\phi_{j,k}^{interv} = \phi_{j,k}, \qquad D < k < 2^j - D - 1$$

(2) on the *edges* of an interval, they are dialations of the boudary adjusted functions:

$$\phi_{j,k}^{interv} = 2^{j/2}\phi_k^{left}(2^j x - k), \qquad 0 \leq k \leq D,$$

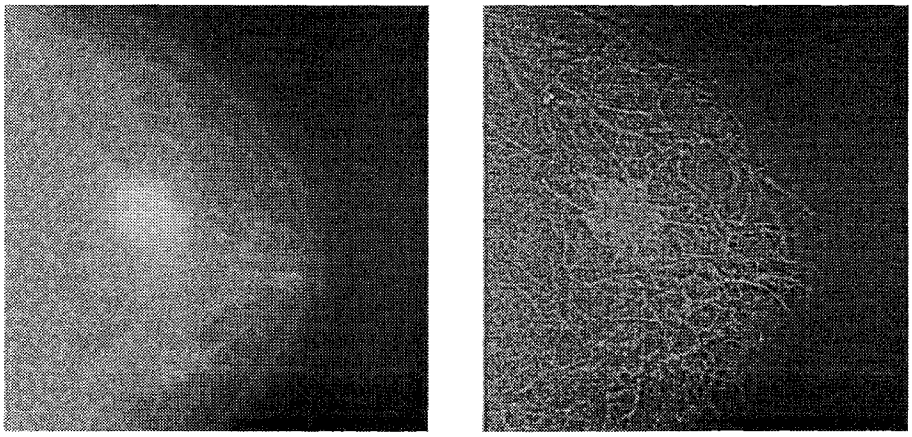

(a)

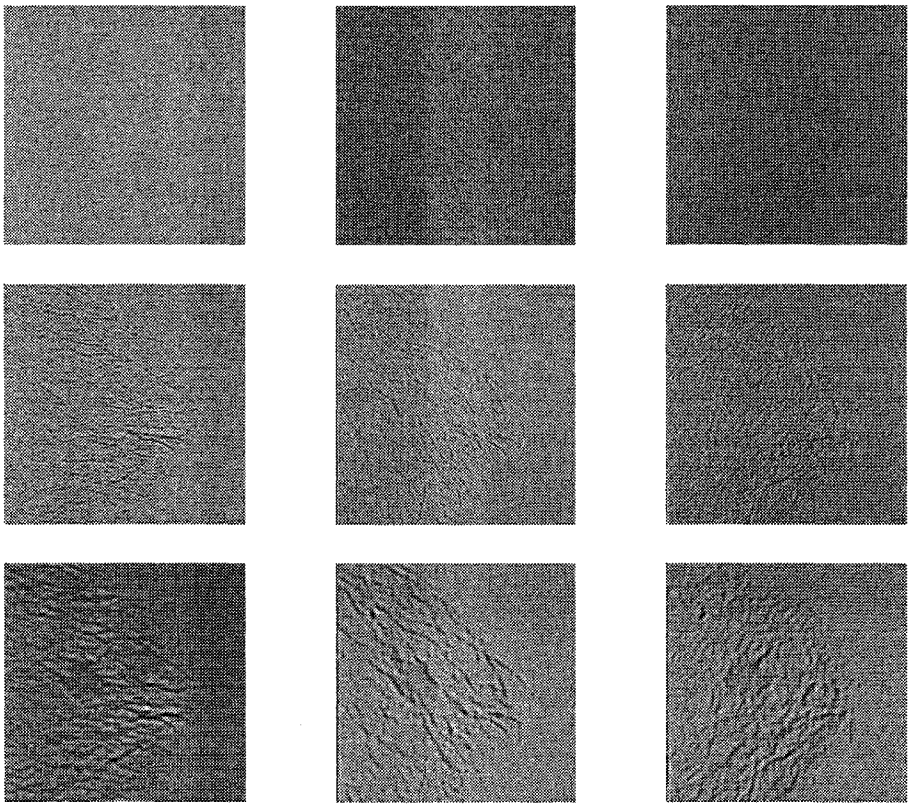

(b)

Figure 4: Processing results: (a) An original mammographic image containing a mass and the enhanced image with borders well defined. (b) The magnitude of filter coefficients for $G(r, \phi - \phi_0)$ at $\{\phi_0\} = \{0, \frac{1}{3}\pi, \frac{2}{3}\pi\}$ (three levels are shown).

$$\phi_{j,2^j-k-1}^{interv} = 2^{j/2}\phi_k^{right}(2^j x - 2^j - k - 1), \qquad 0 \le k \le D.$$

Thus for the spaces $V_j[0,1]$ we can define the functions:

$$\phi_{j,k}^{interv} = \begin{cases} \phi_{j,k}^{left} & 0 \le k \le D \\ \phi_{j,k} & D < k < 2^j - D - 1 \\ \phi_{j,k}^{right} & 2^j - D - 1 \le k \le 2^j. \end{cases}$$

in the same way, we can contruct the wavelets on the interval for the detail spaces $W_j[0,1]$:

$$\psi_{j,k}^{interv} = \begin{cases} \psi_{j,k}^{left} & 0 \le k < \lfloor D/2 \rfloor \\ \psi_{j,k} & \lfloor D/2 \rfloor \le k < 2^j - \lfloor D/2 \rfloor \\ \psi_{j,k}^{right} & 2^j - \lfloor D/2 \rfloor \le k < 2^j. \end{cases}$$

In addition, Donoho [12] showed that if j_0 is a non-negative integer satisfying $2^{j_0} > 2D + 2$ (defining non-interacting boundaries), then there exists a collection of functions $\phi_{j,k}^{interv}$ and $\psi_{j,k}^{interv}$ such that every $f \in \mathbf{C}[0,1]$ has a representation

$$f = \sum_{k=0}^{2^{j_0}-1} s_{j,k}\phi_{j_0,k}^{interv} + \sum_{j \ge j_0} \sum_{k=0}^{2^j-1} d_{j,k}\psi_{j,k}^{interv},$$

with a uniform convergence of partial sums $j \le j_1$ as $j_1 \to \infty$. For a detailed construction of $\phi_{j,k}^{interv}$ and $\psi_{j,k}^{interv}$, please see reference [12].

For processing an arbitrary region within a mammogram, we used a scanline based method: First the rows of a selected ROI were scanned and processed, followed by the colunms. Figures 7(a) and (b) illustrates the interactive selection of a ROI and processing steps.

3.2. ENHANCEMENT TECHNIQUES

To accomplish multiscale contrast enhancement, non-linear techniques for image enhancement were applied to each multiresolution representation. For each basis, there were four components in the transform space: horizontal, vertical, diagonal, and a DC component, represented by d_1^i, d_3^i, d_3^i, s^i respectively, where i is the level of a transform. Let s be the original mammogram, g be the function designed to emphasize features of importance within a selected level i, and L be the number of levels in a transform. Then an enhanced image may be constructed by

$$\hat{s} = \sum_{i=1}^{L} W^{-1}(g(d_1^i), g(d_2^i), g(d_3^i), s^i). \tag{11}$$

In general, by defining a function g, we can denote specific enhancement schemes for modifying the coefficients within distinct levels of scale-space.

3.2.1. Local enancement techniques

A problem for image enhancement in mammography is the ability to emphasize mammographic features while *reducing* the enhancement of noise. Previously [14, 15, 16, 17], we presented a local enhancement technique for digital mammography based on multiscale edges. In this study, enhancement was given by

$$\hat{d}_1^i(m,n) = \begin{cases} d_1^i(m,n), & \text{if } e^i(m,n) \le T^i, \\ g^i\, d_1^i(m,n), & \text{if } e^i(m,n) > T^i, \end{cases}$$

where m and n denote coordinates in the spatial domain, e^i is the edge set corresponding to tranform space component d_1^i, g^i is a local gain, and T^i is a threshold at level i, g^i and T^i are selected adaptively. The edge set e^i of d_1^i is the local maxima of d_1^i along the horizontal direction. For d_2^i and d_3^i, the direction is along the vertical and diagonal orientations (45^o) respectively. Specifically,

$$e^i(m,n) = \begin{cases} |d_1^i(m,n)|, & \text{if } |d_1^i(m,n)| > |d_1^i(m+1,n)| \text{ and} \\ & |d_1^i(m,n)| > |d_1^i(m-1,n)|, \\ 0, & \text{otherwise.} \end{cases}$$

The processing of d_2^i and d_3^i is similar. By replacing d_1^i, d_2^i and d_3^i in Equation (1) with corresponding modified components $\hat{d}_1^i$, $\hat{d}_2^i$ and $\hat{d}_3^i$, we obtained an enhanced image $\hat{s}$.

3.2.2. Multiscale histogram equlization

Histogram equalization of transform space images provides a global method to accomplish multiresolution enhancement. Traditional histogram equlization was applied to each sub-band of coefficients in the transform space (excluding the DC component) to obtain a globally enhanced mamogram.

3.2.3. Multiscale adaptive gain

In this approach, we suppressed pixel values of very small amplitude, and enhanced only those pixels larger than a certain threshold T within each level of transform space. We designed the following function to accomplish this non-linear operation [18]:

$$f(y) = a\left[\text{sigm}(c(y-b)) - \text{sigm}(-c(y+b))\right], \tag{12}$$

where

$$a = \frac{1}{\text{sigm}(c(1-b)) - \text{sigm}(-c(1+b))},$$
$$0 < b < 1,$$

sigm(y) is defined by

$$\text{sigm}(y) = \frac{1}{1+e^{-y}},$$

and, b and c control the threshold and rate of enhancement, respectively. It can be easily shown that $f(y)$ is *continuous* and monotonically increasing within the interval $[-1,1]$ (similar to histogram equalization). Furthermore, a derivative of $f(y)$ of any order exists and is continuous. Therefore, enhancement using $f(y)$ will not introduce any new discontinuities (artifacts).

3.3. EXPERIMENTAL RESULTS AND DISCUSSION

Preliminary results have shown that the multiscale processing techniques described above can make unseen or barely seen features of a mammogram more obvious without requiring additional radiation. Our study suggests that the analyzing functions presented in this paper can improve the visualization of features of importance to mammography and assist the radiologist in the early detection of breast cancer.

Mathematical models of phantoms were constructed to validate our enhancement techniques against false positives arising from possible artifacts introduced by our enhancement methods and evaluate the contrast improvement. Our models included features of regular and irregular shapes and sizes of interest in mammographic imaging, such as microcalcifications, cylindrical and spicular objects, and conventional masses. Techniques for "blending" a normal mammogram with the images of mathematical models were developed. The purpose of these experiments was to test the *performance* of our processing techniques on inputs known "a priori" using mammograms where the objects of interest were deliberately obscured by normal breast tissues. The "imaging" justification for "blending" is readily apparent; a cancer is visible in a mammogram because of its (slightly) higher X-ray attenuation which causes a lower radiation exposure on the film in the appropriate region of a projected image.

Figure 8 shows an example of a mammogram whereby the mathematical phantom shown in Figure 8(a) has been blended into a clinically-proven, cancer-free mammogram. The image shown in Figure 8(b) was constructed by adding the amplitude of the mathematical phantom image to a cancer free mammogram followed by local smoothing of the combined image.

Before applying these techniques, a computer simulated phantom was developed to both characterize and optimize each wavelet based enhancement algorithm [27]. Parameters included the levels of analysis, the threshold (T) and gain (c) parameter value. The phantom study enable us to compute an enhancement factor (EF) which was used to quantitatively measure each algorithms' performance. The EF was defined as the ratio of output to input contrast noise ratio (CNR). The study found that computed EF values correlated well with radiologist feature detection performance.

In addition, radiologists at Shands Hospital at the University of Florida validated that processing the blended mammogram with our local enhancement techniques introduced no significant artifacts and preserved the shapes of the known mammographic features (calcifications, dominant masses, and spicular lesions) contained in the original mathematical phantom.

Enhancement by multiscale edges provided a significant improvement in local contrast for each feature included in the blended mammogram. A quantitative measure of contrast improvement can be defined by a Contrast Improvement Index (CII), $\mathrm{CII} = \frac{C_{\mathrm{Processed}}}{C_{\mathrm{Original}}}$, where $C_{\mathrm{Processed}}$ and C_{Original} are the contrast values for a region of interest in the processed and original images, respectively.

In this paper we adopt a version of the optical definition of contrast introduced by Morrow *et al.* [23]. The contrast C of an object was defined by $C = \frac{f-b}{f+b}$, where f is the mean gray-level value of a particular object in the image, called the *foreground*, and b is the mean gray-level value of a surrounding region called the *background*. This definition of contrast has the advantage of being independent of the actual range of gray levels in the image. We computed local masks to separate the foreground and background regions of each feature included in the blended mammogram.

Figure 8(c) shows the result after processing the blended mammogram with adaptive histogram equalization (AHE). Figure 8(d) was obtained after reconstructing the blended mammogram from interval wavelet transform coefficients modified by multiscale adaptive gain processing (GAIN). Figure 8(e) shows the result after processing the blended mammogram with unsharp masking (UNS). Figures 8(f) shows the result obtained after reconstructing the blended mammogram from interval wavelet transform coefficients modified by multiscale edges (EDGE). Figure 9 shows enlarged areas containing each feature in the processed mammogram for each method of contrast enhancement. The images in each row of Figure 9 were rescaled by the same linear transformation.

Table 1 shows the contrast improvement index (CII) values for the original and enhanced mammographic features shown in Figure 8. From the table we observed that the enhancement by GAIN and EDGE performed significantly better than unsharp masking (UNS) and adaptive histogram equalization (AHE).

Figure 10 shows the improvement of local contrast accomplished by EDGE for a sample scan line profile taken from cross sections of each feature. Note that in all cases contrast was improved while preserving the overall shape of each feature profile.

By using representation of wavelets on the interval, it is possible to enhance arbitrary regions of interest (ROI) within a mammogram. Figure 5(b) shows the enhancement of an arbitrary region of interest using adaptive gain processing of interval wavelet interpolation. Figure 5(c) shows the enhancement of an arbitrary region of interest using multiscale edges.

By constraining the enhancement to only an interest region, computation is greatly reduced (Table 2).

4. SUMMARY

In this study, methods for accomplishing adaptive contrast enhancement by multiscale representations have been investigated. Contrast enhancement was applied to features of specific interest to mammography including masses, spicules and microcalcifications. Multiresolution representations provided an adaptive mechanism for the local emphasis of such features blended into digitized mammograms. In general, improvements in image contrast based on multiscale processing were superior to those obtained using competitive algorithms of unsharp masking and adaptive histogram equalization.

We constructed steerable filters to implement a steerable dyadic wavelet transform. The resulting filter bank ties orientational analysis and multiresolution wavelet representations.

We accomplished image enhancement through nonlinear processing of wavelet coefficients at distinct scales and orientations. We have shown our results in the context of digital mammography, however, these techniques may be applied to other imaging modalities as well.

Deslauriers-Dubuc interpolation representations on an interval enabled us to enhance arbitrary regions of interest (Fig. 5). This can provide radiologists an interactive capability for enhancing only suspicious regions of a mammogram. It also reduces the computational cost compared to processing an entire mammogram. These initial results are encouraging and suggest that wavelet based image processing algorithms could play an important role in improving the imaging performance of digital mammography screening.

5. REFERENCES

[1] W. T. Freeman and E. H. Adelson, "The design and use of steerable filters," *IEEE Trans. Pattern Anal. Machine Intell.*, vol. PAMI-13, pp. 891–906, 1991.

[2] P. Perona, "Deformable kernels for early vision," in *Proc. IEEE Comput. Soc. Conf. Comput. Vision and Pattern Recogn.*, pp. 222–227, Maui, 1991.

[3] D. Shy and P. Perona, "X-Y separable pyramid steerable scalable kernels," in *Proc. IEEE Comput. Soc. Conf. Comput. Vision and Pattern Recogn.*, pp. 237–244, Seattle, 1994.

[4] E. P. Simoncelli, W. T. Freeman, E. H. Adelson, and D. J. Heeger, "Shiftable multiscale transforms," *IEEE Trans. Inform. Theory*, vol. IT-38, pp. 587–607, 1992.

[5] S. Mallat and S. Zhong, "Characterization of signals from multiscale edges," *IEEE Trans. Pattern Anal. Machine Intell.*, vol. PAMI-14, pp. 710–732, 1992.

[6] J. Lim, *Two-Dimensional Signal and Image Processing.* Englewood Cliffs, NJ: Prentice Hall, 1990.

[7] A. F. Laine, J. Fan, and S. Schuler, "A Framework for Contrast Enhancement by Dyadic Wavelet Analysis," *Second International Workshop on Digital Mammography*, York, UK, July 10-12, 1994.

[8] A. Cohen, I. Daubechies, "Wavelets on the interval and fast wavelet transforms," *Applied and Computational Harmonic Analysis*, Vol. 1, No. 1, 1993.

[9] B. Jawerth, W. Sweldens, "An overview of wavelet based multiresolution analyses," *SIAM Review*, vol. 36, no. 3, pp. 377–412, 1994.

[10] L. S. Davis, A. Rosenfield, "Noise cleaning by iterated local averaging," *IEEE Transactions on Systems, Man and Cybernetics,* Vol. SMC-8, pp. 705–710, 1978.

[11] G. Deslauriers, S. Dubuc, "Symmetric iterative interpolation process," *Constructive Approximation*, vol. 5, pp. 49–68, 1989.

[12] D. L. Donoho, "Smooth wavelet decomposition with blocky coefficient kernels," *Recent Advances in Wavelet Analysis*, pp. 1–43, Academic Press , Inc., Boston, 1994.

[13] S. Dubuc, "Interpolation through an iterative scheme," *J. Math. Anal. and Appl.*, vol. 114, pp. 185–204, 1986.

[14] A. Laine, "Multiscale wavelet representations for mammographic feature analysis," *Image Enhancement Techniques: Computer Science, National Cancer Institute Breast Imaging Workshop: State-of-the-Art and New Technologies*, Bethesda, MD, September 1991.

[15] A. Laine, S. Song, "Multiscale wavelet representations for mammographic feature analysis," in *Proceedings of SPIE: Conference on Mathematical Methods in Medical Imaging*, San Diego, CA, July 23–25, 1992.

[16] A. Laine, S. Song, "Wavelet processing techniques for digital mammography," in *Proceedings of SPIE: Conference on Visualization in Biomedical Computing,* Chapel Hill, NC, October 13–16, 1992.

[17] A. Laine, S. Song, J. Fan, "Adaptive Multiscale Processing for Contrast Enhancement," to appear in *Proceedings of SPIE: Conference on Biomedical Imaging and Biomedical Visualization,* San Jose, CA, January 31–February 4, 1993.

[18] A. Laine, S. Schuler, J. Fan, W. Huda, "Mammographic Feature Enhancement by Multiscale Analysis," *IEEE Transactions on Medical Imaging,* Vol. 13(4), December, 1994.

[19] S. Mallat, "A Theory for Multiresolution Signal Decomposition: The Wavelet Representation," *IEEE Transactions on Pattern Analysis and Machine Intelligence,* Vol. 11(7), pp. 674–693, 1989.

[20] S. Mallat, "Multiresolution approximations and wavelet orthonormal bases of L^2(R)," *Transactions of the American Mathematical Society,* Vol. 315(1), pp. 69–87, 1989.

[21] S. Mallat, "Multifrequency channel decompositions of images and wavelet models," *IEEE Transactions on Acoustics, Speech, and Signal Processing,* Vol. ASSP-37(12), pp 2091–2110, 1989.

[22] S. Mallat, S. Zhong, "Signal characterization from multiscale edges," in *10th International Conference on Pattern Recognition,* Atlantic City, New Jersey, June 1990.

[23] W. M. Morrow, R.B. Paranjape, R.M. Rangayyan, J.E.L. Desautels. Region-based contrast enhancement of mammograms. *IEEE Transactions on Medical Imaging.* Vol. 11(3): 392–406, 1992.

[24] M. Nagao, T. Matsuyama, "Edge preserving smoothing," *Computer Graphics and Image Processing*, Vol. 9, pp. 394–407, 1979.

[25] A. Scheer, F.R.D. Velasco, A. Rosenfiled, "Some new image smoothing techniques," *IEEE Transactions on Systems, Man and Cybernetics,* Vol. SMC-10(3): pp. 153–158, 1980.

[26] P.G. Tahoces, J. Correa, M. Souto, C. Gonzalez, L. Gomez, J. Vidal, "Enhancement of chest and breast radiographs by automatic spatial filtering," *IEEE Transaction on Medical Imaging,* Vol. MI-10(3), pp. 330–335, 1991.

[27] Y. Xing, W. Huda, A. Laine, "Simulated phantom images for optimizing wavelet based image processing algorithms in mammography", *Proceedings of SPIE-The International Society for Optical Engineering*, Vol. 2299, pp. 207-217, July, 1994.

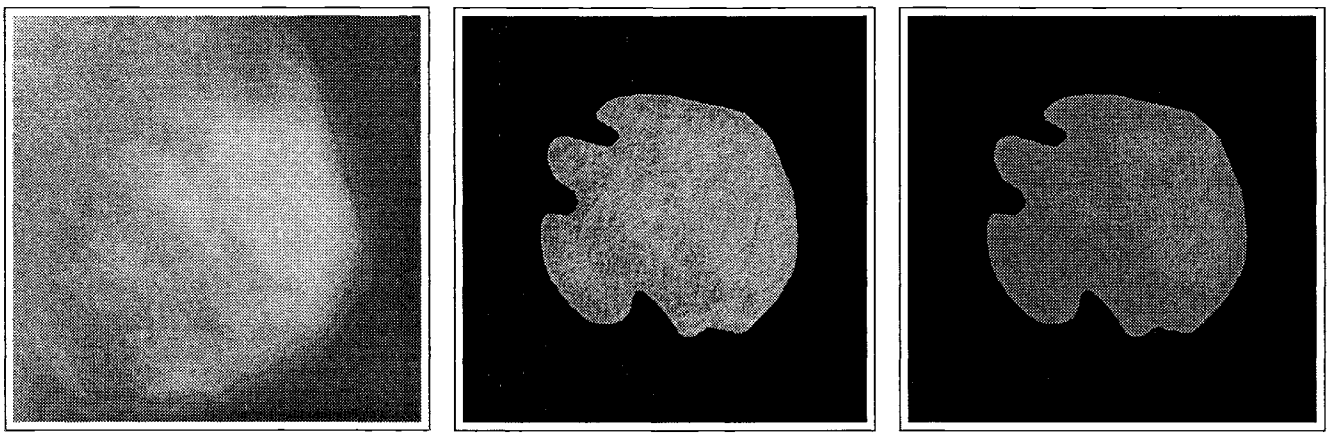

(a) (b) (c)

Figure 5: Blended mammogram: (a) Original mammogram blended with mathematical phantom. (b) ROI enhancement by adaptive gain processing of DD wavelet coefficients. (c) ROI enhancement by multiscale edges of DD interpolation.

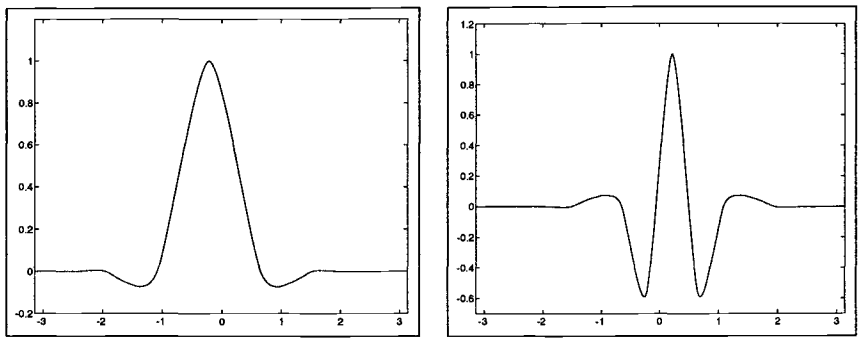

(a) (b)

Figure 6: (a) Refinement relation for Deslauries-Dubuc interpolation. (b) Interval wavelet plot, $D = 3$.

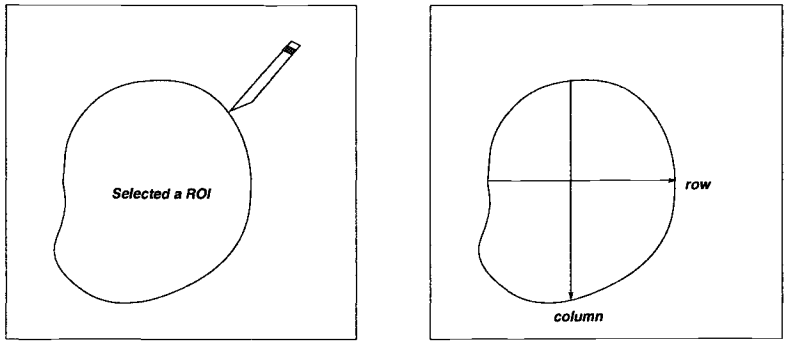

(a) (b)

Figure 7: (a) Selected ROI within a mammogram, (b) ROI is processed based on tensor product: each row is processed first, followed by the processing of each column.

Table 1: CII for enhancement by unsharp masking (UNS), adaptive histogram equalization (AHE), and by local enhancement of multiscale edges obtained from Deslauriers-Dubuc interpolation (EDGE), adaptive gain processing of Deslauriers-Dubuc interpolation (GAIN).

Feature	CII_{UNS}	CII_{AHE}	CII_{GAIN}	CII_{EDGE}
Minute microcalcification cluster	1.3294	0.8442	7.7949	12.7298
Microcalcification cluster	3.6958	4.9759	10.9217	11.0783
Spicular lesion	2.0174	3.5714	12.5714	13.7596
Circular (arterial) calcification	2.1888	4.4601	8.0160	10.6941
Well-circumscribed mass	1.4857	31.1714	9.8286	11.3429

Table 2: Comparison of computation time. $T_{Entire-mammogram}$ represents the time to process an whole mammogram, while T_{ROI} represents the time to process only a selected ROI. The number of pixels within the ROI shown in Figure 12 was 76267 (Program was executed on Sun Sparc station 10/30).

Computation time (in seconds) comparison of whole mammogram vs ROI			
Matrix size (number of pixels)	$T_{Entire-mammogram}$	T_{ROI}	$T_{Entire-mammogram}/T_{ROI}$
512x512	748	135	5.54
1024x1024	5760	135	42.67

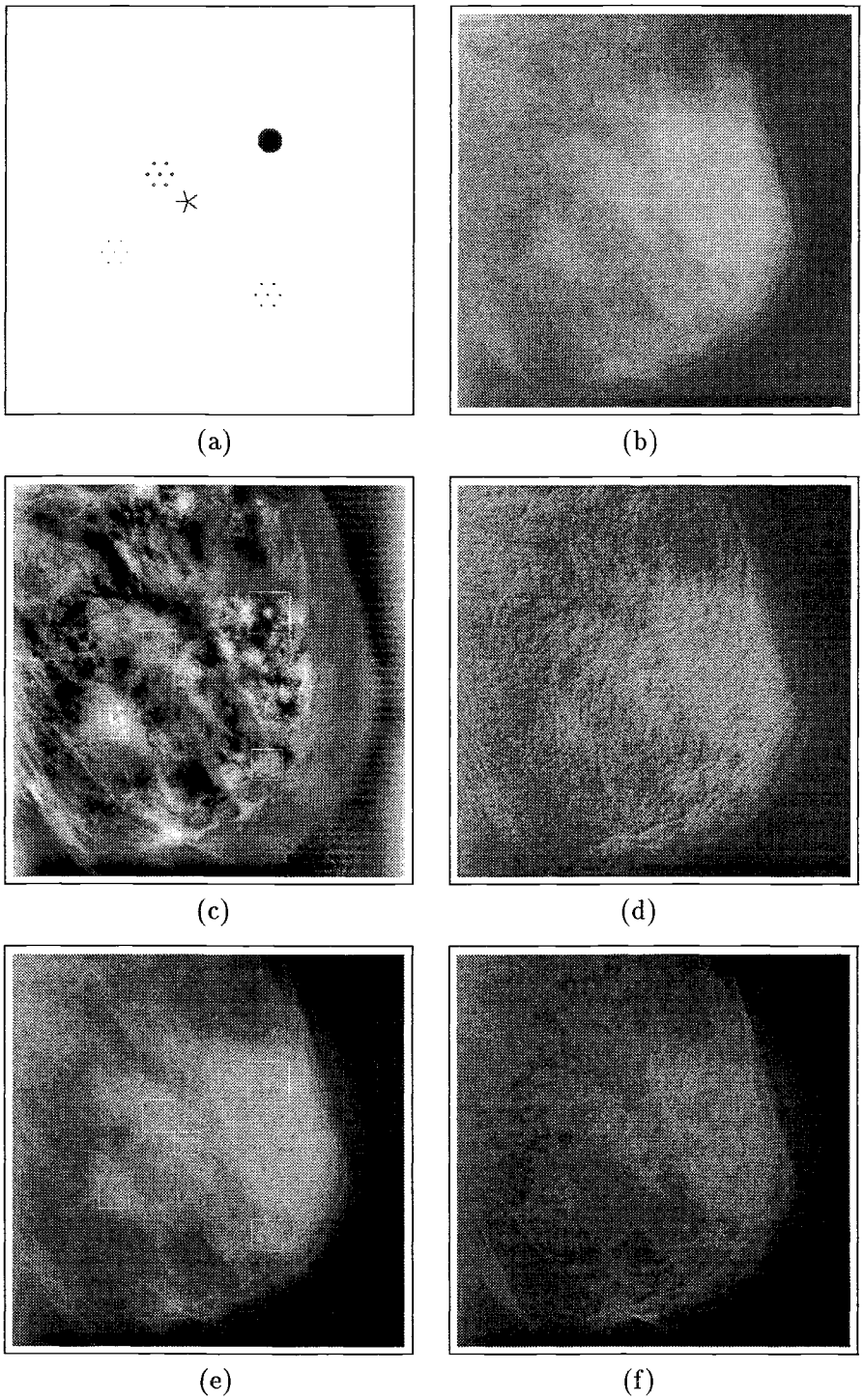

Figure 8: (a) Mathematical phantom. (b) Mammogram M56 blended with phantom image. (c) Enhancement by adaptive histogram equalizaiton. (d) Enhancement by adaptive gain processing of DD interpolation coefficients. (e) Enhancement by traditional unsharp masking. (f) Enhancement by multiscale edges of DD interpolation coefficients.

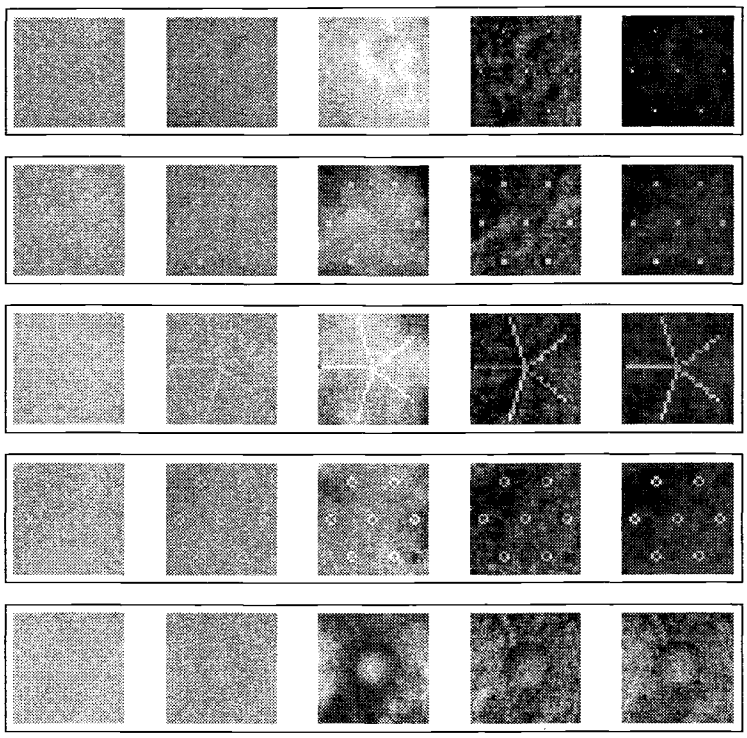

(a) (b) (c) (d) (e)

Figure 9: Contrast enhancement of features in blended mammogram. Phantom mammographic features from top to bottom: minute microcalcification cluster, microcalcification cluster, spicular lesion, circular (arterial) calcification, and a well-circumscribed mass. (a) Original image. (b) Enhancement by unsharp masking. (c) Enhancement by adaptive histogram equalization. (d) Enhancement by adaptive gain processing of DD wavelet coefficients. (e) Local enhancement by multiscale edges of DD wavelet coefficients.

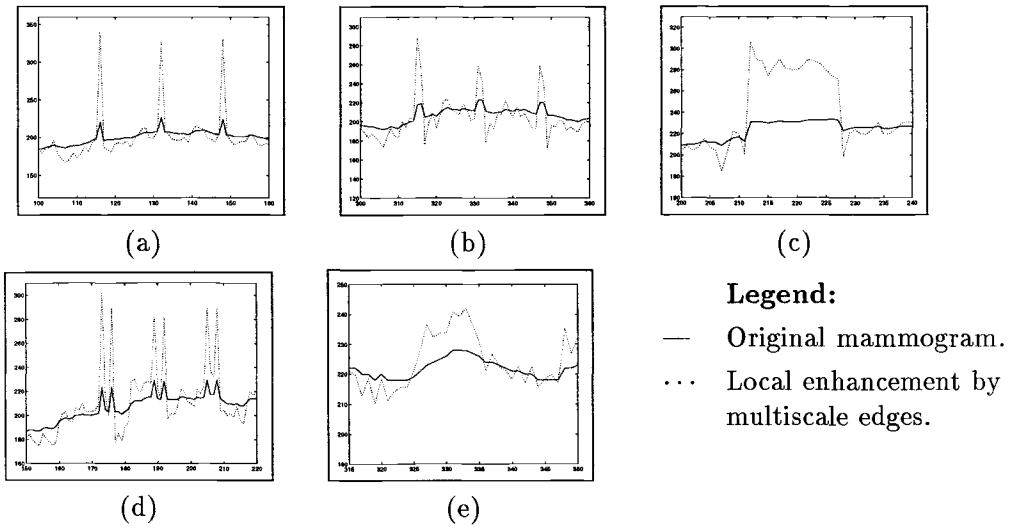

Figure 10: Sample scan lines displaying enhancement by the method of multiscale edges of DD wavelet coefficients: (a) minute microcalcification cluster, (b) microcalcification cluster, (c) spicular lesion, (d) circular (arterial) calcification and (e) well-circumscribed mass.